An Alternatively Spliced Gain-of-Function NT5C2 Isoform Contributes to Chemoresistance in Acute Lymphoblastic Leukemia

Manuel Torres-Diz[1], Clara Reglero[2], Catherine D. Falkenstein[3], Annette Castro[1], Katharina E. Hayer[1,4], Caleb M. Radens[5,6], Mathieu Quesnel-Vallières[6], Zhiwei Ang[1], Priyanka Sehgal[1], Marilyn M. Li[7,8], Yoseph Barash[5,6], Sarah K. Tasian[3,9], Adolfo Ferrando[2,10], and Andrei Thomas-Tikhonenko[1,3,5,8,9]

ABSTRACT

Relapsed or refractory B-cell acute lymphoblastic leukemia (B-ALL) is a major cause of pediatric cancer–related deaths. Relapse-specific mutations do not account for all chemotherapy failures in B-ALL patients, suggesting additional mechanisms of resistance. By mining RNA sequencing datasets of paired diagnostic/relapse pediatric B-ALL samples, we discovered pervasive alternative splicing (AS) patterns linked to relapse and affecting drivers of resistance to glucocorticoids, antifolates, and thiopurines. Most splicing variations represented cassette exon skipping, "poison" exon inclusion, and intron retention, phenocopying well-documented loss-of-function mutations. In contrast, relapse-associated AS of *NT5C2* mRNA yielded an isoform with the functionally uncharacterized in-frame exon 6a. Incorporation of the 8-amino acid sequence SQVAVQKR into this enzyme created a putative phosphorylation site and resulted in elevated nucleosidase activity, which is a known consequence of gain-of-function mutations in *NT5C2* and a common determinant of 6-mercaptopurine resistance. Consistent with this finding, NT5C2ex6a and the R238W hotspot variant conferred comparable levels of resistance to 6-mercaptopurine in B-ALL cells both *in vitro* and *in vivo*. Furthermore, both NT5C2ex6a and the R238W variant induced collateral sensitivity to the inosine monophosphate dehydrogenase inhibitor mizoribine. These results ascribe to splicing perturbations an important role in chemotherapy resistance in relapsed B-ALL and suggest that inosine monophosphate dehydrogenase inhibitors, including the commonly used immunosuppressive agent mycophenolate mofetil, could be a valuable therapeutic option for treating thiopurine-resistant leukemias.

Significance: Alternative splicing is a potent mechanism of acquired drug resistance in relapsed/refractory acute lymphoblastic leukemias that has diagnostic and therapeutic implications for patients who lack mutations in known chemoresistance genes.

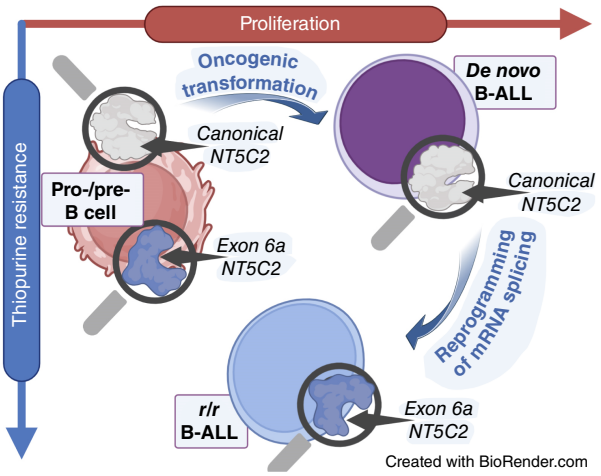

Introduction

Leukemia is the most common cancer in children and adolescents/young adults, accounting for almost one thirds of all pediatric cancers, with the majority of cases classified as B-cell acute lymphoblastic leukemia (B-ALL). Only ~50% of children with first relapse survive in the long term, and outcomes are appreciably poorer with subsequent relapses. Early bone marrow (BM) relapses occurring within 3 years of diagnosis are particularly difficult to salvage (1). As a result, relapsed or refractory (r/r) high-risk B-ALL cases account for a substantial number of pediatric cancer–related

[1]Division of Cancer Pathobiology, Children's Hospital of Philadelphia, Philadelphia, Pennsylvania. [2]Institute for Cancer Genetics, Columbia University, New York, New York. [3]Division of Oncology, Children's Hospital of Philadelphia, Philadelphia, Pennsylvania. [4]Department of Biomedical and Health Informatics, Children's Hospital of Philadelphia, Philadelphia, Pennsylvania. [5]Cell and Molecular Biology Graduate Group, University of Pennsylvania, Philadelphia, Pennsylvania. [6]Department of Genetics, Perelman School of Medicine at the University of Pennsylvania, Philadelphia, Pennsylvania. [7]Division of Genomic Diagnostic, Children's Hospital of Philadelphia, Philadelphia, Pennsylvania. [8]Department of Pathology and Laboratory Medicine, Perelman School of Medicine at the University of Pennsylvania, Philadelphia, Pennsylvania. [9]Department of Pediatrics, Perelman School of Medicine at the University of Pennsylvania, Philadelphia, Pennsylvania. [10]Department of Pediatrics, Columbia University, New York, New York.

Corresponding Author: Andrei Thomas-Tikhonenko, Pathology and Lab Medicine, Children's Hospital of Philadelphia, 3056 Colket Translational Research Building, 3501 Civic Center Blvd, Philadelphia, PA 19104-4399. E-mail: andreit@pennmedicine.upenn.edu

Cancer Res 2024;84:3327–36

doi: 10.1158/0008-5472.CAN-23-3804

deaths. In addition, although most cases of B-ALL are diagnosed early in life, most deaths from B-ALL (~80%) occur in adults, largely due to r/r disease. Indeed, adults with B-ALL experience very high relapse rates and long-term event-free survival of less than 50% (2, 3).

What molecular mechanisms are responsible for treatment failures in r/r B-ALL is only partially understood. Previous whole-exome/genome sequencing efforts have identified a dozen of recurrent mutations in relapse-specific targets (4–6). Some of them (e.g., *TP53*) are known to mediate responses to pan-cancer drugs such as anthracyclines, whereas others are involved in therapeutic responses to specific leukemia therapeutics: glucocorticoids (*NR3C1* and *WHSC1*), antifolates (*FPGS*), and thiopurines (*PRPS1*, *PRPS2*, and *NT5C2*). The most recent effort to catalog such mutations yielded up to 50 genes significantly enriched at first relapse but often as subclonal or low-recurrence events (7). Even the most recurrently affected drivers are mutated in fewer than 20% of all samples, suggesting a major role for alternative mechanisms of gene dysregulation. One such mechanism is alternative spicing (AS); however, its role in acquired resistance to chemotherapy remains poorly defined.

To bridge this gap, we previously had generated and mined new and existing RNA sequencing (RNA-seq) datasets in search for local splicing variations (LSV) prevalent in B-ALL samples but rare in normal BM cell counterparts. Of note, B-ALL–specific AS was found to affect 15 out of the 20 top leukemia driver genes from the COSMIC database with frequencies far exceeding those of somatic mutations (8). This intersection suggests that AS could be an important mechanism of both leukemogenesis and drug resistance. Here, we provide evidence that a subset of relapses often lacking identifiable acquired mutations has an AS signature simultaneously affecting multiple r/r B-ALL drivers. Among them is a novel *NT5C2* exon 6a mRNA variant encoding a gain-of-function nucleotidase isoform with increased enzymatic activity capable of conferring resistance to 6-mercaptopurine (6-MP).

Materials and Methods

Splicing analysis

The Modeling Alternative Junction Inclusion Quantification (MAJIQ) algorithm version 4.4 (RRID:SCR_016706; ref. 9) was run, with each sample being quantified individually, on a build comprising 219 TARGET B-ALL samples with *de novo* junction detection but without intron retention detection, as described previously (10–13). Samples were run against the GENCODE hg38 quantification. For ΔPSI (percent spliced-in) quantification, the MAJIQ PSI and Voila tools were used on 48 diagnostic–relapse paired samples to extract all the LSVs in all the samples with the –show-all flag. Visualization and downstream analyses were conducted in R using the ggplot2 (RRID:SCR_014601), ComplexHeatmap (RRID:SCR_017270), and tidyverse (RRID:SCR_019186) packages. The sashimi plots were generated with the ggsashimi tool. In parallel, raw junction-spanning reads were obtained from the STAR aligner (see Supplementary Materials) and expressed as junction counts per million. Junction counts per millions for select AS events in select samples are included in Supplementary Table S1.

ONT-based targeted long-read sequencing

For each target gene, primers corresponding to first and last exons were designed to ensure full coverage of relevant AS events. Typically, 5 ng of cDNA were amplified with LongAmp Taq 2× Master Mix (New England Biolabs) for 25 cycles. The resulting amplicons were subjected to amplicon-seq [#SQK-NBD114.24, Oxford Nanopore Technologies (ONT)] library preparation. Subsequently, each library was loaded into a Spot-ON flow cell version R10 (#FLO-MIN114, ONT) and sequenced in a MinION Mk1C device (ONT) until at least 1,000 reads per sample were obtained. The results were aligned using Minimap2 version 2.24-r1122 (RRID:SCR_018550) and visualized in Integrative Genomics Viewer (RRID:SCR_011793) version 2.12.3.

Cell lines and cell culture

REH (RRID:CVCL_1650), Nalm-6 (RRID:CVCL_0092), 697 (RRID:CVCL_0079), and MHH-CALL-4 (RRID:CVCL_1410) human B-ALL cell lines originally obtained from commercial repositories were cultured and maintained in conditions recommended by ATCC or Deutsche Sammlung von Mikroorganismen und Zellkulturen (DSMZ). Cell line authentication for REH and MHH-CALL-4 was performed by short tandem repeat profiling. All cell lines were routinely subjected to Sartorius EZ-PCR Mycoplasma Detection Kit testing.

Genome editing

Single-guide RNAs targeting CREBBP exons 25 and 26 and CAS9 protein were obtained from Integrated DNA Technologies (see Supplementary Materials). Cas9 ribonucleoprotein complexes were assembled following manufacturing recommendations. These ribonucleoprotein complexes were transfected into 697 and REH cells via electroporation using the Neon transfection system (Invitrogen Neon Transfection System Model MPK5000) and Neon 10 μL Transfection Kit (#MPK1096, Invitrogen) using the following conditions: 1,700 V, 20 ms, and 2 pulses. Their effects on exon removal were measured by cDNA PCR, with primers amplifying the region between exons 20 and 27 (see Supplementary Materials), and Western blotting.

MO treatment

For FPGS splice switching, a specific Vivo-morpholino (MO) targeting the canonical 3′ splice site of exon 8 was designed (AAATTCCACTGGTCCGTCTGACCCC). As a control, the reverse sequence was used in order to maintain sequence composition, as recommended by the manufacturer. Cells were incubated with 2.5 μmol/L MOs for 24 hours before treatment with methotrexate (MTX).

Plasmid constructs and viral infections

For NT5C2 constructs, the coding sequence of the canonical *NT5C2* isoform (NM_001351169.2) was amplified using specific primers (see Supplementary Materials) and cloned into the pLVX backbone (Clontech) modified with the EF1a promoter and the basticidin-resistant gene using NEBuilder HiFi DNA Assembly Master Mix (New England Biolabs). Specific primers and NEBuilder HiFi DNA Assembly Master Mix were used to introduce exon 6a or the R238W mutation into the canonical sequence of *NT5C2*. For viral particle production, 293T cells (ATCC) grown to 90% confluence in a 10-cm Petri dish were transfected with 10 μg of the NT5C2 constructs, 2.5 μg of the pMD2.G (#12259, Addgene), and 7.5 μg of the psPAX2 (#12260, Addgene) using 60 μL of 25 μmol/L polyethylenimine (PEI) transfection reagent (#24765, Polysciences). Supernatants were collected 48 hours after transfection, passed through 0.45-μm PVDF filters, and incubated for 48 hours with 4 ×

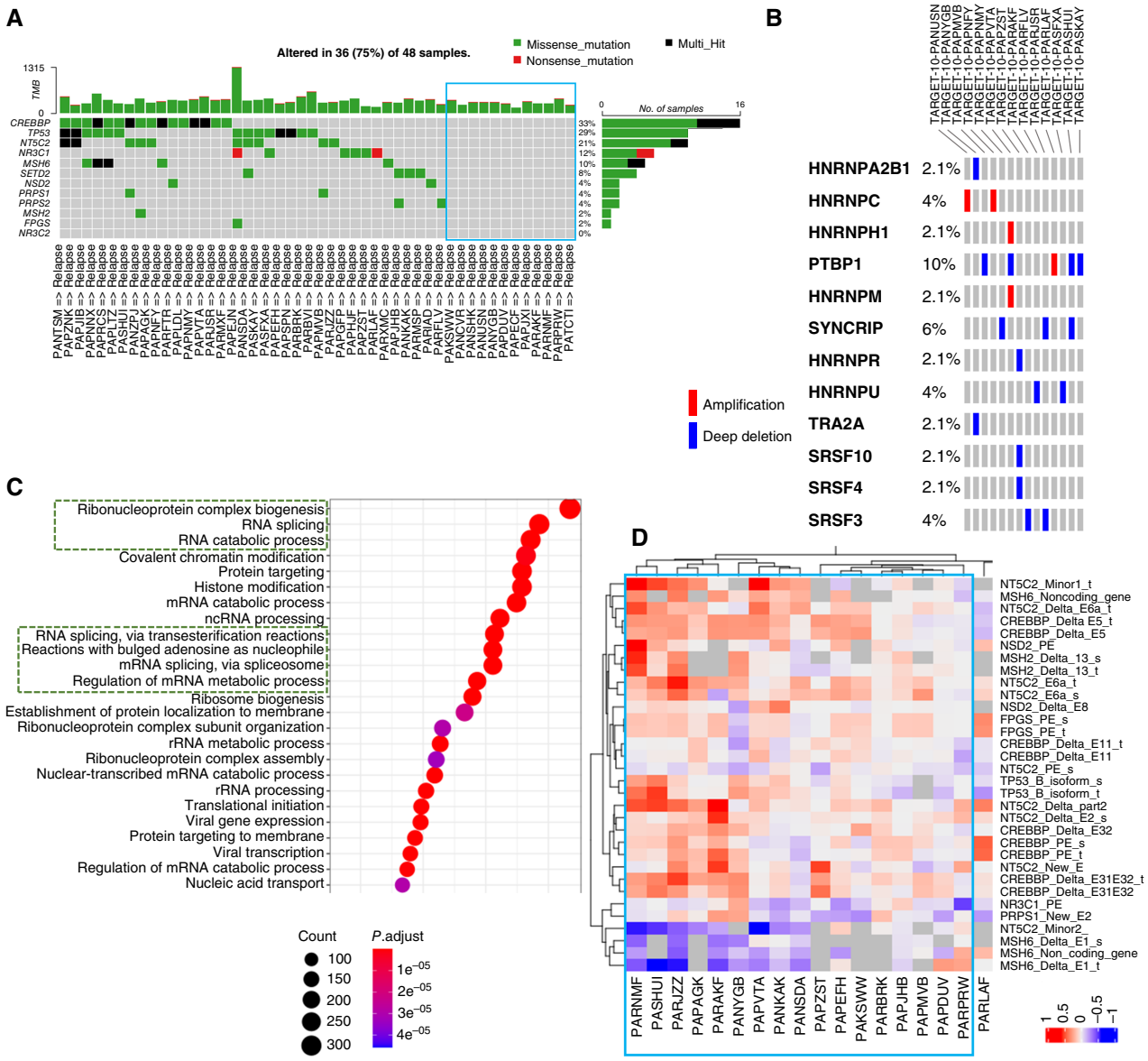

Figure 1.

Splicing signature of relapsed leukemias. **A,** Oncoprint showing distribution of acquired mutations in known r/r genes in 48 paired TARGET samples. The blue rectangle on the right marks samples with no identifiable relapse-specific mutations. **B,** Oncoprint showing distribution of mutations in select SF genes in 48 TARGET patients under investigation. **C,** Gene set enrichment analysis of transcripts comprising one of the unsupervised clusters. Green rectangles, Gene Ontology categories involving RNA splicing. **D,** Heatmap showing changes in splicing in a cluster of 17 relapse vs. diagnostic B-ALL samples (light blue box). The dendrograms on top represent the results of unsupervised clustering without excluding samples with known relapse-specific mutations. The adjacent sample PARLAF with several profoundly mis-spliced transcripts is shown for comparison. Red and blue, increases/decreases in inclusion of exonic segments, respectively.

10^6 cells in media containing 10 μg/mL polybrene (#HY-112735, MedChemExpress). After 48 hours, culture media were replaced, and cells were incubated with 10 μg/mL blasticidin for 96 hours.

NT5C2 recombinant protein production and purification

Recombinant wild-type (WT) and mutant NT5C2 constructs were cloned, expressed, and purified as previously described (14). Briefly, the full-length *NT5C2* cDNA constructs with N-terminal hexahistidine (His6) tags were inset into the pET28a-LIC expression vector. Recombinant proteins were expressed in Rosetta 2 (DE3) *E. coli* cells by induction with 0.5 mmol/L isopropyl-β-D-thio-galactopyranoside overnight at 16°C. Then recombinant proteins were purified using an ÄKTA fast protein liquid chromatography system (GE Healthcare). This was followed by affinity and size-exclusion chromatographies.

5′-Nucleotidase assays

5′-Nucleotidase activities of purified WT and mutant NT5C2 proteins were measured in the absence and presence of allosteric activators using a 5′-NT enzymatic test kit (Diazyme) according to the manufacturer's instructions, as described previously (15). All assays were performed in triplicate and analyzed using a GloMax multidetection system plate reader (Promega).

In vitro killing assay

For treatments with MTX (#S1210, Selleck Chemicals), 6-MP (#852678-5G-A, Sigma Aldrich), mizoribine (#S1384, Selleck Chemicals), doxorubicin (#HY-15142, MedChemExpress), dexamethasone (#D4902, Sigma-Aldrich), and vincristine (#HY-N0488, MedChemExpress), cells were incubated with increasing concentrations of each drug for 72 hours. Vehicle control dilutions corresponding to the highest drug concentration were used as a baseline measure for 100% survival. Cell viability was measured by CellTiter-Glo assays (G7572, Promega) following the manufacturer's instructions. IC_{50} values were calculated using Prism software v9.3.1 (GraphPad software) with the log (inhibitor) versus normalized response–variable slope.

In vivo cell line xenograft animal studies

Luciferase-transduced REH cells were transduced with NT5C2 WT, E6a, or R238W constructs and selected with blasticidin for 96 hours. Following selection, NOD/SCID/Il2rgtm1wjl/SzJ (NSG) mice were intravenously injected with 1×10^6 parental or modified REH cells and assessed for leukemia engraftment using the Xenogen *In Vivo* Imaging System. Ten days after B-ALL engraftment was detected, cohorts of mice ($n = 5$/group) of each REH cell type were randomized for treatment with vehicle control or 6-MP (100 mg/kg/day). 6-MP was administered intraperitoneally daily × 5 days, as described previously (16). Radiance as a surrogate for total leukemia burden was measured by *in vivo* bioluminescent imaging of mice following i.p. injection of luciferin substrate. Bioluminescent imaging assessment was performed with Living Image software (PerkinElmer) with statistical analysis and data display performed using Prism (GraphPad).

Data availability

Main RNA-seq datasets analyzed in this study were parts of the TARGet alL phase I and II projects (https://portal.gdc.cancer.gov/projects) and the BLUEPRINT consortium (http://dcc.blueprint-epigenome.eu). TARGET datasets accessed through dbGaP were phs000463.v23.p8 ALL Pilot Phase 1 and phs000464.v23.p8 ALL Expansion Phase 2. The raw long-read sequencing data generated in this study are publicly available in the Sequence Read Archive as Project PRJNA1138448. All other raw data generated in this study are available upon request from the corresponding author.

Results

A subset of r/r B-ALL has an AS signature affecting multiple chemoresistance genes

To gain new insights into molecular mechanisms that render B-ALL chemotherapy ineffective, we analyzed 48 TARGET patients with available paired diagnosis–relapse (D-R) RNA-seq datasets. We called mutations in known r/r driver genes from the RNA-seq data using Genome Analysis Toolkit (see Supplementary Materials). In agreement with prior analyses, we observed that in 12 out of 48 D-R pairs (25%), there were no identifiable relapse-specific mutations in 12 common r/r genes (**Fig. 1A**). To determine whether differential gene expression could account for the chemoresistant phenotype, we performed principal component analysis on all 96 samples. We observed no separation of diagnostic and relapse samples (Supplementary Fig. S1A, red and cyan dots, respectively), suggesting that differential gene expression as a whole is not a primary driver of B-ALL relapses. However, pervasive AS reported in our earlier B-ALL study (8) could contribute to chemoresistance by altering expression levels of distinct mRNA isoforms. Thus, we asked whether any members of the HNRNP and SRSF/TRA2 superfamilies of splicing factors (SF) strongly implicated in exon inclusion/skipping are affected by mutations or copy number alterations (CNA). Using cBioPortal (17), we identified such CNAs in 14 out of 48 patients (30%). For example, deep deletions of both SRSF4 and SRSF10 genes was found in patient PAPZST and the SRSF3 gene in samples PARAKF and PARJSR (**Fig. 1B**). Of note, these deletions affected only the latest among longitudinal samples, attesting to their possible role in B-ALL relapses.

To explore the extent and functional consequences of splicing dysregulation, we ran the MAJIQ 2.1 splicing algorithm on paired diagnostic/relapse samples while filtering for LSVs with ≥20% difference in junction inclusion with 95% confidence (Supplementary Fig. S1B). We further filtered for samples without known driver mutations and for LSVs affecting these unmutated driver genes. After performing hierarchical clustering, we discovered a cluster of five relapses with concurrent missplicing of multiple chemoresistance genes (Supplementary Fig. S1C, light blue rectangle). To elucidate the underlying molecular mechanisms, we performed gene set enrichment analysis (18) on all transcripts differentially expressed in D-R pairs in that cluster of patients. Top 3 and 7 out of top 12 categories pertained to RNA splicing (**Fig. 1C**). To determine whether AS is only in active in samples with unmutated drivers of chemoresistance or has a broader impact, we extended MAJIQ splicing analysis to all 48 D-R pairs. Unsupervised clustering rediscovered the same 5 patient samples and assigned additional 12 r/r leukemias to the same cluster for the total of 17 (**Fig. 1D**, light blue rectangle), potentially implicating AS in ∼1/3 of B-ALL relapses. We obtained further evidence of SF dysregulation at the level of poison exon inclusion known to result in nonsense-mediated decay (19). For example, in all relapse samples, almost 100% of transcripts encoding the aforementioned SRSF10 carried stop codon–containing exon 3a, presumably rendering them nonfunctional (Supplementary Fig. S1D).

We then considered more carefully the nature of AS events contributing to this cluster (**Table 1**). We noted that many of them mapped to genes conferring resistance to commonly used B-ALL therapeutics: glucocorticoids (*NR3C1*), thiopurines (*PRPS1* and *NT5C2*), and antifolates (*FPGS*). In additional, they affected relapse genes associated with more general, not exclusively cancer cell–intrinsic mechanisms. Examples included the master epigenetic regulator *CREBBP* and its functional interactor *SETD2* and the universal pan-cancer suppressor *TP53*. Overall, the majority of the splicing variants in **Table 1** are putative loss-of-function events as they either directly disrupt open reading frames (mimicking nonsense mutations) or render the transcript vulnerable to nonsense-mediated decay. For instance, *TP53* exon 9i contains a premature stop codon, and its inclusion results in the previously validated p53β protein isoform with multiple functional defects (20, 21). However, the effects of *CREBBP* exon

Table 1. r/r B-ALL drivers affected by AS.

Gene Name	Junctions coordinates (hg38)	Affected exons (MANE v1.0 nomenclature)	Effect on protein
CREBBP	**3736815-3739578**	**Δex26**	**In-frame truncation**
CREBBP	**3736815-3740399**	**Δex25-26**	**In-frame truncation**
CREBBP	3745595-3749627 3745354-3745440	"Poison" exon 21a inclusion	Nonsense-mediated decay
CREBBP	3774693-3778011	Δex11	In-frame truncation
CREBBP	3782926-3793386	Δex5	In-frame truncation
FPGS	**127807775-127808234**	**ex8 alt 5′ site**	**Frameshift**
MSH2	47475270-47478272	Δex13	Frameshift
MSH6	47696097-47708183 47696097-47698818	Alt 5′UTR	Noncoding isoforms
MSH6	47737506-47790927	Δex1	Loss of AUG
NR3C1	143396525-143399656	Novel Δex2a	Early termination
NSD2	1935262-1939654	Δex8	Frameshift
NSD2	1952231-1952752	int11 retention	No-coding transcript
NT5C2	103100943-103101045	int8 retention	Frameshift
NT5C2	**103105381-103105706**	**Novel exon 6a** (previously referred to as exon 4a in ref. 8)	**In frame insertion**
NT5C2	103143168-103174858	Novel exon 3a	Unknown
NT5C2	103174982-103193236	Δex2	Shorter 5′UTR
NT5C2	103106706-103174858	Δex4	Frameshift
NT5C2	103111805-103174858	alt ex3 5′ site/alt exon 4a	Minor isoform
NT5C2	103111805-103139406	alt exon 4a	Minor isoform
PRPS1	107628750-107630017	Novel exon 1a	Early termination
TP53	7673339-7673535	Novel exon 9a	Hypomorphic β isoform

NOTE: Events in bold are under investigation in this study.

25/26 skipping and the alternative 5′ splice site in *FPGS* exon 8 (previously reported in the literature; refs. 22, 23) could not be inferred *a priori* in the context of the loss-of-function model and required experimental investigation.

AS events affecting *CREBBP* and *FPGS* transcripts in r/r B-ALL are loss of function

Although *CREBBP* mRNA was affected by several AS events, in-frame skipping of exons 25 and 26 was of potential functional significance as it removes 261bp (87aa) from the HAT domain. This AS event was also among the most robust in our analysis of B-ALL relapses: on average, 50% of all *CREBBP* reads aligned to the ex24-ex27 junction (**Fig. 2A**). In the representative example in **Fig. 2B**, fewer than 30% of reads mapped uniquely to the Δex25/26 isoform in the diagnostic sample (32 reads in the blue sashimi plots), whereas in the paired relapse sample, this event predominated (99 reads in the red sashimi plots). To determine the effects of this event on protein function, we designed two sets of single-guide RNAs mapping to the exons in question and used them to remove the exon 25 to 26 segment from 697 B-ALL cells via CRISPR-mediated genome editing. Using semiquantitative RT-PCR, we detected decreased expression of the *CREBBP* full-length isoform and robust skipping of its exons 25 and/or 26, with combined skipping of both exons being the most readily detectable event (**Fig. 2C**). This was also apparent when protein levels were analyzed by immunoblotting (**Fig. 2D**, top). Because the splicing event affects the HAT domain, we chose, as a functional readout, its effects on histone modifications. We observed that *CREBBP* exon 25/26 skipping resulted in a commensurate reduction in H3K27Ac while preserving total H3 levels (**Fig. 2D**). These results support the notion that *CREBBP* exon 25/26 skipping yields a protein isoform deficient in histone acetyl transferase activity.

The AS event affecting *FPGS* exon 8 was equally pervasive: only in a few pairs of samples was its direction reversed (**Fig. 2E**). In a representative relapse sample depicted in **Fig. 2F**, 65% of reads connected to the downstream exon 9 (186 in the red sashimi plot) originated at the alternative 5′ splice site, whereas in the paired diagnostic sample, this ratio was flipped (32 reads in the blue sashimi plot). To model this event *in vitro*, we designed a MO antisense splice blocker targeting the canonical 5′ splice site, thus forcing the use of the alternative downstream site (see Materials and Methods). In transfected Nalm6 B-ALL cells, this MO almost completely redirected splicing toward the expected downstream site, resulting in partial intron inclusion and rendering exon 8 "poisonous" via inclusion of a stop codon ("PE" in **Fig. 2G**). Therefore, the use of *FPGS* MO also resulted in a sharp decrease in FPGS protein levels, as evidenced by immunoblotting (**Fig. 2H**). As FPGS is a known driver of sensitivity to MTX (24), we tested the effects of MO-induced *FPGS* AS on cell survival in response to this antifolate drug. In these experiments, redirecting splicing of *FPGS* exon 8 toward the downstream splice site resulted in essentially complete resistance to MTX and unattainable IC_{50} values (**Fig. 2I**). These data solidified our conclusion that AS phenocopies loss-of-function mutations in this gene previously linked to chemoresistance in r/r B-ALL (5).

AS of *NT5C2* yields an mRNA isoform conferring resistance to thiopurines

Across all relapse-associated AS events identified in our analysis (**Table 1**), the alternative isoform of *NT5C2* with the functionally uncharacterized in-frame exon 6a (previously referred to by us as exon 4a; ref. 8) stood out. This microexon is annotated in RefSeq, and its robust inclusion was detected in normal BM B-cell progenitors in our earlier AS study (8) and in some other populations of

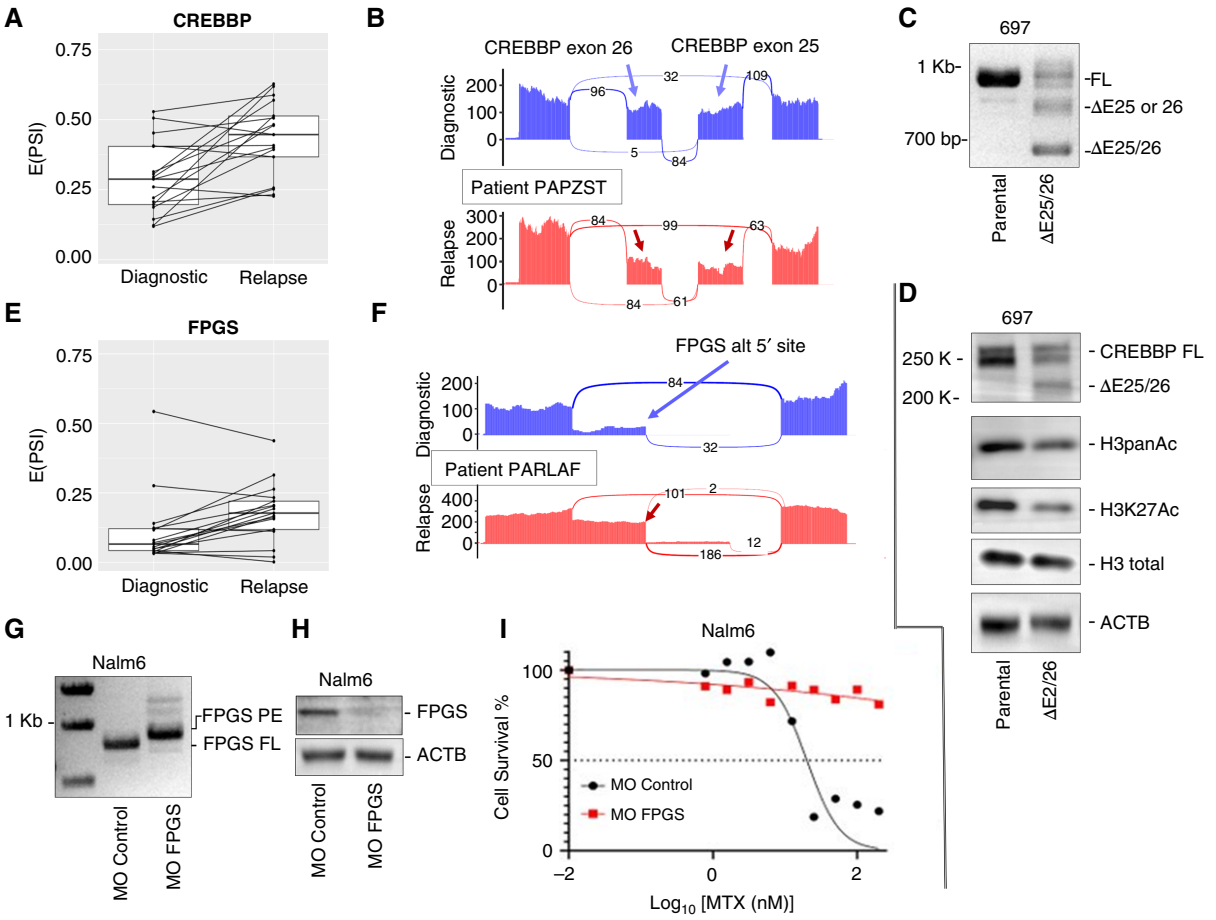

Figure 2.

LOF AS events affecting *CREBBP* and *FPGS* transcripts. **A,** Box plot showing percentages of reads connecting *CREBBP* exon 24 to exon 27 in diagnosis/relapse pairs from **Fig. 1D**. PSI, percent spliced-in. **B,** Sashimi plots visualizing the same *CREBBP* events in a representative PAPZST sample. **C,** RT-PCR analysis of *CREBBP* transcripts in 697 B-ALL cells transfected with exons 25- and 26-specific single-guide RNAs packaged into Cas9 particles. **D,** Immunoblotting analysis of the same samples using antibodies recognizing indicated proteins and post-translational modifications of histone H3. β-Actin was used as a loading control. **E,** Box plot showing percentages of reads connecting the 5′ splice site in *FPGS* exon 8 to the downstream exon 9 in diagnosis/relapse pairs from **Fig. 1D**. **F,** Sashimi plots visualizing the same *FPGS* event in a representative PARLAF sample. **G,** RT-PCR analysis of *FPGS* transcripts in Nalm6 cells transfected with control or *FPGS* exon 8 5′ splice site-specific MO. **H,** Immunoblotting analysis of the same samples using an anti-FPGS antibody. **I,** IC_{50} plot representing survival of these cells after exposure to increasing concentrations of MTX. FL, full-length isoform; PE, poison exon-containing isoform.

hematopoietic cells in our recently unveiled MAJIQlopedia, a reference database for splicing variations across human cancers and normal tissues (25). However, it is not included in the Matched Annotation from the NCBI and EMBL-EBI (MANE), which is a broadly used standard for clinical reporting. Of note, increased frequencies of this event were observed in most relapsed B-ALL samples compared with the matched diagnostic specimens (**Fig. 3A**). In a representative relapse sample depicted in **Fig. 3B**, >80% of reads originating in the upstream canonical exon 6 (352 in the red sashimi plot) connected to exon 6a, whereas in the paired diagnostic sample, <25% did (80 in the blue sashimi plot). This finding was consistent with our prior data showing lower levels of *NT5C2* exon 6a inclusion in *de novo* leukemias compared with their normal BM progenitors (8).

To determine whether *NT5C2* exon 6a can be found in translatable cap-to-poly(A) protein-coding transcripts, we amplified its cDNA and subjected the resultant 1.7-kb fragment (Supplementary Fig. S2A) to targeted resequencing using the ONT approach (see Materials and Methods). Using this assay, we readily detected exon *NT5C2* 6a inclusion in the majority of reads corresponding to the Philadelphia chromosome–like MHH-CALL4 cell line with the *IGH*::*CRLF2* rearrangement (Supplementary Fig. S2B). Further support for the translatability of this isoform comes from its inclusion in the UniProt database (accession code: A0A6Q8PHP0) and the inclusion of the exon 6a–encoded tryptic peptide SQVAVQKR in PeptideAtlas (accession code: PAp02559851).

Inclusion of exon 6a in the *NT5C2* open reading frame results in the addition of eight extra amino acids near the ATP-binding effector site 2. To determine the effect of this alteration on NT5C2 function, we produced the corresponding recombinant protein (Supplementary Fig. S2C and S2D) and tested its enzymatic activity in nucleotidase assays with IMP as a substrate under basal conditions and following allosteric activation with ATP (14). In these cell-

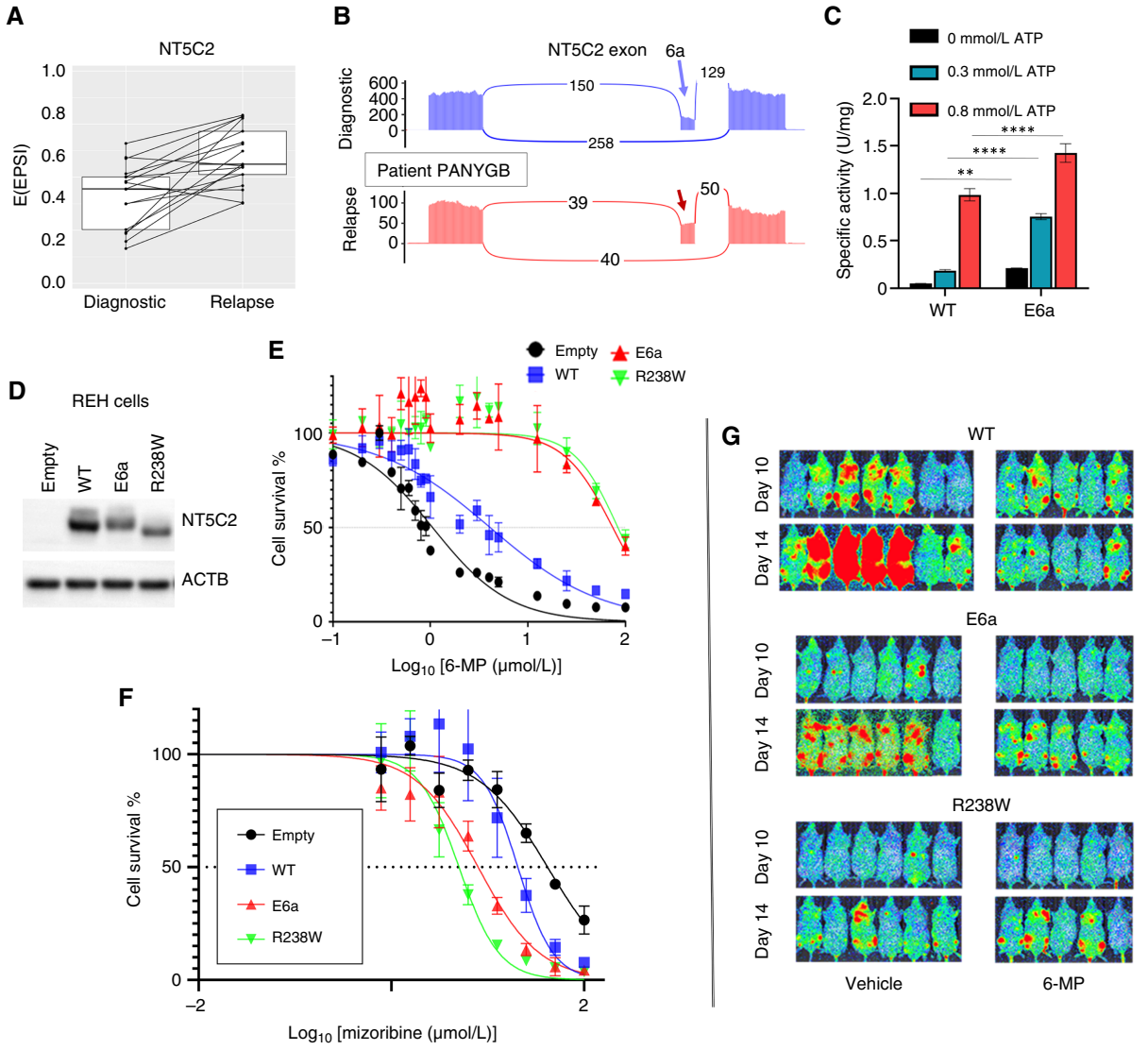

Figure 3.

The NT5C2ex6a isoform as a driver of resistance to thiopurines. **A,** Box plot showing percentage of read connecting *NT5C2* exon 6 to exon 6a in six diagnosis/relapse pairs depicted in **Fig. 1C**. PSI, percent spliced-in. **B,** Sashimi plots visualizing the same *NT5C2* events in a representative PANYGB sample. **C,** *In vitro* nucleotidase assays assessing the enzymatic activity of the canonical (WT) and E6a NT5C2 isoforms in the presence of increasing concentrations of ATP. Data are shown as the mean ± SD. Asterisks indicate statistical significance per Student *t* test, with *P* values calculated using two-way ANOVA. **, $P < 0.0058$; ****, $P < 0.0001$. **D,** Expression levels of transduced NT5C2 isoforms in REH cells. WT, E6a, and R238W denote the canonical isoform, the NT5ex6a splice variant, and the R238W hotspot mutant, respectively. Empty, vector-only cells. **E,** The IC_{50} plot representing survival of these cells exposed to increasing concentrations of 6-MP. **F,** The IC_{50} plot representing survival of these cells exposed to increasing concentrations of mizoribine. **G,** Bioluminescent detection of the same cells additionally expressing the firefly luciferase gene. Cells were xenografted into NSG mice and imaged on days 10 and 14.

free assays, bacterially produced NT5C2ex6a exhibited elevated enzymatic activity compared with canonical NT5C2 protein in response to low concentrations of ATP (**Fig. 3C**). This biochemical response was consistent with a gain of function mechanism, similar to that observed for most relapsed-associated *NT5C2* mutations characterized to date (14).

To rigorously test a potential role of *NT5C2* ex6a in 6-MP resistance, we generated REH B-ALL cell models expressing canonical *NT5C2*, *NT5C2* ex6a, and *NT5C2* R238W, a validated gain-of-function resistance driver with the most common hotspot mutation (**Fig. 3D**; ref. 14). Cell viability assays carried out with increasing concentrations of 6-MP demonstrated that expression of the *NT5C2* ex6a isoform confers 6-MP resistance comparable to that induced by the *NT5C2* R238W mutation and well above that conferred by the canonical isoform of WT *NT5C2* (**Fig. 3E**; Supplementary Fig. S2E), although the effects were somewhat less potent in Nalm-6 cells (Supplementary Fig. S2F). Metabolically, increased enzymatic activity of NT5C2 mutants results in increased clearance of thiopurine mononucleotide monophosphate metabolites but also in depletion of intracellular nucleotide pools, which in turn renders leukemia

cells more sensitive to mizoribine, an inosine monophosphate dehydrogenase inhibitor (16). Therefore, we evaluated the relationship between *NT5C2* ex6a and sensitivity to this drug. Once again, both *NT5C2* R238W-expressing and *NT5C2* ex6a-expressing cells showed convergent phenotypes with respect to increased sensitivity to mizoribine treatment *vis-a-vis* cells expressing the canonical isoform of WT *NT5C2* (**Fig. 3F**; Supplementary Fig. S2G).

We further noted that the NT5C2 exon 6a–encoded peptide SQVAVQKR contains a characteristic SQ motif, which constitutes the recognition site for the DNA-PK/ATR/ATM subfamily of kinases of the PIKK family (26), also reflected in the Kinase Library (27). This observation suggested a potential role for protein phosphorylation at this site in the regulation of NT5C2 activity. Thus, we generated mutant variants of *NT5C2* ex6a, in which the ex6a-encoded serine residue was replaced by the common phosphomimetic aspartic acid (S131D) or by alanine (S131A) to serve as a phosphorylation-deficient control. Evaluation of responses to 6-MP treatment of REH cells expressing each of these constructs revealed that whereas the parental NT5C2 E6a isoform and its S131A derivative conferred equivalent levels of 6-MP resistance, the S131D substitution resulted in the markedly increased resistance phenotype, with one log further increase in the IC_{50} value (Supplementary Fig. S2H). These results suggest that phosphorylation events at the S131 site might augment *NT5C2* exon 6a–driven 6-MP resistance.

To directly assess the impact of *NT5C2* ex6a inclusion on leukemia cells growth and therapy responses *in vivo*, we implanted luciferase-expressing REH cells expressing the canonical WT *NT5C2* isoform, *NT5C2* R238R, and *NT5C2* ex6a into NSG mice and imaged animals on days 5, 8, 12, and 14. Previous reports linked hyperactive NT5C2 to a "fitness cost" phenotype and decreased cell proliferation resulting from the depletion of intracellular nucleotide pools (16). Consistent with these observations, expression of *NT5C2* R238W and *NT5C2* ex6a induced clear growth retardation when compared with expression of the canonical *NT5C2* isoform (Supplementary Fig. S3A). Nevertheless, we observed robust leukemia engraftment, allowing us to test the effect of the three different *NT5C2* variants on chemotherapy response by treating each experimental group with either vehicle or 6-MP (**Fig. 3G**). When compared with the initial treatment timepoint (day 10 after engraftment), the WT model shows a negative fold change (FC; plotted on the *y*-axis in Supplementary Fig. S3B), which was indicative of cell death. In contrast, the E6a model demonstrates slower cell division under treatment, but the FC remains nonnegative, signifying that the treatment does not induce cell death. Notably, the E6a model exhibits an identical FC to the R238W mutant model. These findings further support the comparable roles of these two NT5C2 variants in promoting chemoresistance.

Discussion

RNA-centric regulatory mechanisms, such as formation of fusion transcripts and circular RNAs, RNA editing, and in particular aberrant mRNA splicing, recently have been recognized as key drivers of neoplastic growth (28). Indeed, mutations in genes encoding core SFs (SF3B1, SRSF2, etc.) are common in adult leukemias, raising the possibility that targeting aberrant splicing programs could be a viable therapeutic option. Although such mutations are exceedingly rare in pediatric AML and ALL, a growing body of work by us and other researchers has revealed that inclusion of "poison" and other noncanonical exons in SF-encoding transcripts is among the most consistent splicing aberration in both B-ALL and T-ALL (8, 29), as well as in many solid tumors (19, 30). Additionally, we show that in TARGET r/r B-ALL samples, SRSF- and HNRNP-encoding genes are frequently affected by CNAs such as deep deletions, likely exacerbating AS.

We also report pervasive dysregulation, at the level of mRNA splicing, of key chemosensitivity genes. In most cases (*CREBBP*, *FPGS*, and other examples in **Table 1**) the AS events are of the loss-of-function nature, making it challenging to devise pharmacologic interventions. Still, an RNA-based diagnostic test detecting, for example, the heavy usage of FPGS ex8 alt 5′ site could guide clinical decisions regarding the use of MTX. Thus, we envision that targeted RNA-seq panels, either short- or long-read, will become valuable companion diagnostics, despite known limitations of underlying technologies (31).

The case of NT5C2 is particularly interesting from the therapeutic standpoint since *NT5C2* splicing aberrations leading to the inclusion of cryptic exon 6a ultimately create a proteoform with gain-of-function properties. Since gain-of-function NT5C2 variants interfere with cell proliferation (16), it comes as no surprise that the inclusion of *NT5C2* exon 6a is actually reduced in *de novo* leukemias compared with pro-B cells (8) and is regained only upon treatment with thiopurines as a trade-off between survival and proliferation. This complex dynamic was apparent in our *in vivo* experiments, in which both NT5C2 E6a and R238W leukemias grew more slowly in NSG mice than the controls but effectively resisted treatment with 6-MP. Of interest, at least in one leukemia variant (PARJZZ), *NT5C2* exon 6a inclusion coexists with the hotspot mutation R367Q reported earlier (4). This finding is consistent with an evolutionary model wherein nonmutational mechanisms (AS, NT5C2 phosphorylation) confer initial resistance to 6-MP, enable persistence of proliferating cells, and allow eventual emergence of clones with gain-of-function NT5C2 mutations and a constitutive resistance phenotype.

Robust expression of the NT5C2ex6a isoform not only predicts resistance to thiopurines but may suggest additional therapeutic options, such as treatment with the emerging class of direct NT5C2 small-molecule inhibitors such as CRCD2 (32) and also with clinically used inosine monophosphate dehydrogenase inhibitors and immunosuppressive agents mycophenolate mofetil and mizoribine (33). In support of this notion, NT5C2ex6a-expressing REH and NALM6 cells were found to exhibit heightened sensitivity to mizoribine compared with the isogenic cell lines reconstituted with the canonical NT5C2 isoform.

Other ways to therapeutically target NT5C2 dysregulation are likely to exist. Our recently published work elucidated the role of NT5C2 post-transcriptional modification in chemoresistance, with phosphorylation of the Ser-502 residue by a yet-to-be-identified protein kinase increasing its activity against 6-MP (32). Our current data showing that substituting Ser at position 131 with a phosphomimetic Asp augments NT5C2ex6a-induced resistance to 6-MP lend further credence to the model linking NT5C2 phosphorylation and chemoresistance functions. If future research confirms the involvement of ATR/ATM family kinases in phosphorylating the NT5C2 exon 6a-encoded SQ motif, a variety of small-molecule inhibitors of these enzymes (34) will be available for preclinical studies and clinical trials aiming to resensitize r/r B-ALL to chemotherapy and in doing so improve outcomes in this aggressive and often fatal childhood cancer.

Authors' Disclosures

M. Torres-Diz reports a patent for PCT/US2023/025031 pending. C. Reglero reports her work was supported by a Leukemia and Lymphoma Society Special Fellow award. M.M. Li reports personal fees from Bayer HealthCare Pharmaceuticals Inc. and Agilent Technologies outside the submitted work. Y. Barash reports grants from the NIH during the conduct of the study and grants from the NIH, CureBRCA, and Basser Institute outside the submitted work. MAJIQ 2.0 used in this study is available for licensing for free for academics and for a fee for commercial usage. Some of the commercial licensing revenue goes to Y. Barash and members of the Barash laboratoy. A. Ferrando reports grants from the NIH, Leukemia and Lymphoma Society, Alex's Lemonade Stand Foundation, and Irving Institute for Clinical and Translational Research of Columbia University during the conduct of the study and other support from Regeneron Pharmaceuticals outside the submitted work; in addition, A. Ferrando has a patent for NT5C2 inhibitors issued. A. Thomas-Tikhonenko reports grants from the NIH, Pennsylvania Department of Health, St. Baldrick's Foundation, Stand Up To Cancer (SU2C), The V Foundation for Cancer Research, The Emerson Collective, and Alex's Lemonade Stand Foundation during the conduct of the study and grants from CureSearch for Childhood Cancer, Pfizer ASPIRE Onc/Hem Program and personal fees from the University of Miami, the Italian Association for Cancer Research, Guidepoint, and Houston Methodist outside the submitted work; in addition, A. Thomas-Tikhonenko has a patent for PCT/US2023/025031 pending. No disclosures were reported by the other authors.

Authors' Contributions

M. Torres-Diz: Conceptualization, data curation, formal analysis, validation, investigation, writing–original draft, writing–review and editing. **C. Reglero:** Investigation. **C.D. Falkenstein:** Investigation. **A. Castro:** Investigation. **K.E. Hayer:** Data curation, formal analysis. **C.M. Radens:** Data curation, formal analysis. **M. Quesnel-Vallières:** Data curation, formal analysis. **Z. Ang:** Conceptualization, writing–review and editing. **P. Sehgal:** Resources. **M.M. Li:** Conceptualization. **Y. Barash:** Conceptualization, data curation, formal analysis. **S.K. Tasian:** Supervision. **A. Ferrando:** Conceptualization, supervision, writing–review and editing. **A. Thomas-Tikhonenko:** Conceptualization, supervision, funding acquisition, writing–original draft, project administration, writing–review and editing.

Acknowledgments

The authors are grateful to past and present members of the Barash, Tasian, and Thomas-Tikhonenko laboratories and Penn's RNA Club for many helpful discussions. This work was supported by grants from the NIH/NCI (U01 CA232563 to A. Thomas-Tikhonenko and Y. Barash, U01 CA232486 and U01 CA243072 to S.K. Tasian, and P30 CA013696, R35 CA210065, and CA216981 to A. Ferrando), Pennsylvania Department of Health SFY22 CURE Non-Formula Collaborative Research on Childhood and Adolescent Blood Cancers (#67-173 to A. Thomas-Tikhonenko), U.S. Department of Defense (CA180683P1 to S.K. Tasian), St. Baldrick's Foundation [EPICC Team and St. Baldrick's SU2C Dream Team Translational Cancer Research Grant (SU2C-AACR-DT-27-17) to A. Thomas-Tikhonenko and S.K. Tasian], The V Foundation for Cancer Research (T2018-014 to A. Thomas-Tikhonenko), The Emerson Collective (886246066 to A. Thomas-Tikhonenko), Alex's Lemonade Stand Foundation (Innovation Awards to ATT and AF), and Leukemia & Lymphoma Society (Translational Research Grant 6455-15 and Screen to Lead Grant 8011-18 to A. Ferrando). The indicated SU2C research grant is administered by the AACR, the scientific partner of SU2C. C. Reglero is a past Special Fellow and S.K. Tasian is a Scholar of the Leukemia & Lymphoma Society. A. Thomas-Tikhonenko and A. Ferrando acknowledge support from the SPROUT Program and Accelerating Cancer Therapeutics Program at CHOP and Columbia University, respectively. M. Torres-Diz and A. Thomas-Tikhonenko further acknowledge support from The Ellen Weisberg Fund: Advancing Breakthroughs in Pediatric Cancer. S.K. Tasian is Joshua Kahan Endowed Chair in Pediatric Leukemia Research, and A. Thomas-Tikhonenko is Mildred L. Roeckle Endowed Chair in Pathology at Children's Hospital of Philadelphia.

Note

Supplementary data for this article are available at Cancer Research Online (http://cancerres.aacrjournals.org/).

Received April 9, 2024; revised June 11, 2024; accepted July 25, 2024; published first August 2, 2024.

References

1. Hunger SP, Raetz EA. How I treat relapsed acute lymphoblastic leukemia in the pediatric population. Blood 2020;136:1803–12.
2. Roberts KG, Mullighan CG. Genomics in acute lymphoblastic leukaemia: insights and treatment implications. Nat Rev Clin Oncol 2015;12:344–57.
3. Jeha S, Choi J, Roberts KG, Pei D, Coustan-Smith E, Inaba H, et al. Clinical significance of novel subtypes of acute lymphoblastic leukemia in the context of minimal residual disease-directed therapy. Blood Cancer Discov 2021;2:326–37.
4. Ma X, Edmonson M, Yergeau D, Muzny DM, Hampton OA, Rusch M, et al. Rise and fall of subclones from diagnosis to relapse in pediatric B-acute lymphoblastic leukaemia. Nat Commun 2015;6:6604.
5. Li B, Brady SW, Ma X, Shen S, Zhang Y, Li Y, et al. Therapy-induced mutations drive the genomic landscape of relapsed acute lymphoblastic leukemia. Blood 2020;135:41–55.
6. Oshima K, Khiabanian H, da Silva-Almeida AC, Tzoneva G, Abate F, Ambesi-Impiombato A, et al. Mutational landscape, clonal evolution patterns, and role of RAS mutations in relapsed acute lymphoblastic leukemia. Proc Natl Acad Sci U S A 2016;113:11306–11.
7. Waanders E, Gu Z, Dobson SM, Antić Ž, Crawford JC, Ma X, et al. Mutational landscape and patterns of clonal evolution in relapsed pediatric acute lymphoblastic leukemia. Blood Cancer Discov 2020;1:96–111.
8. Black KL, Naqvi AS, Asnani M, Hayer KE, Yang SY, Gillespie E, et al. Aberrant splicing in B-cell acute lymphoblastic leukemia. Nucleic Acids Res 2018;46:11357–69.
9. Vaquero-Garcia J, Barrera A, Gazzara MR, González-Vallinas J, Lahens NF, Hogenesch JB, et al. A new view of transcriptome complexity and regulation through the lens of local splicing variations. Elife 2016;5:e11752.
10. Sotillo E, Barrett DM, Black KL, Bagashev A, Oldridge D, Wu G, et al. Convergence of acquired mutations and alternative splicing of CD19 enables resistance to CART-19 immunotherapy. Cancer Discov 2015;5:1282–95.
11. Zheng S, Gillespie E, Naqvi AS, Hayer KE, Ang Z, Torres-Diz M, et al. Modulation of CD22 protein expression in childhood leukemia by pervasive splicing aberrations: implications for CD22-directed immunotherapies. Blood Cancer Discov 2022;3:103–15.
12. Yang SY, Hayer KE, Fazelinia H, Spruce LA, Asnani M, Black KL, et al. FBXW7β isoform drives transcriptional activation of the proinflammatory TNF cluster in human pro-B cells. Blood Adv 2023;7:1077–91.
13. Ang Z, Paruzzo L, Hayer KE, Schmidt C, Torres Diz M, Xu F, et al. Alternative splicing of its 5′-UTR limits CD20 mRNA translation and enables resistance to CD20-directed immunotherapies. Blood 2023;142:1724–39.
14. Dieck CL, Tzoneva G, Forouhar F, Carpenter Z, Ambesi-Impiombato A, Sánchez-Martín M, et al. Structure and mechanisms of NT5C2 mutations driving thiopurine resistance in relapsed lymphoblastic leukemia. Cancer Cell 2018;34:136–47.
15. Tzoneva G, Perez-Garcia A, Carpenter Z, Khiabanian H, Tosello V, Allegretta M, et al. Activating mutations in the NT5C2 nucleotidase gene drive chemotherapy resistance in relapsed ALL. Nat Med 2013;19:368–71.
16. Tzoneva G, Dieck CL, Oshima K, Ambesi-Impiombato A, Sánchez-Martín M, Madubata CJ, et al. Clonal evolution mechanisms in NT5C2 mutant-relapsed acute lymphoblastic leukaemia. Nature 2018;553:511–4.
17. Cerami E, Gao J, Dogrusoz U, Gross BE, Sumer SO, Aksoy BA, et al. The cBio cancer genomics portal: an open platform for exploring multidimensional cancer genomics data. Cancer Discov 2012;2:401–4.
18. Subramanian A, Tamayo P, Mootha VK, Mukherjee S, Ebert BL, Gillette MA, et al. Gene set enrichment analysis: a knowledge-based approach for interpreting genome-wide expression profiles. Proc Natl Acad Sci U S A 2005;102:15545–50.
19. Thomas JD, Polaski JT, Feng Q, De Neef EJ, Hoppe ER, McSharry MV, et al. RNA isoform screens uncover the essentiality and tumor-suppressor activity of ultraconserved poison exons. Nat Genet 2020;52:84–94.

20. Bourdon JC, Fernandes K, Murray-Zmijewski F, Liu G, Diot A, Xirodimas DP, et al. p53 isoforms can regulate p53 transcriptional activity. Genes Dev 2005; 19:2122–37.
21. Tang Y, Horikawa I, Ajiro M, Robles AI, Fujita K, Mondal AM, et al. Downregulation of splicing factor SRSF3 induces p53β, an alternatively spliced isoform of p53 that promotes cellular senescence. Oncogene 2013;32:2792–8.
22. Stark M, Wichman C, Avivi I, Assaraf YG. Aberrant splicing of folylpolyglutamate synthetase as a novel mechanism of antifolate resistance in leukemia. Blood 2009;113:4362–9.
23. Wojtuszkiewicz A, Raz S, Stark M, Assaraf YG, Jansen G, Peters GJ, et al. Folylpolyglutamate synthetase splicing alterations in acute lymphoblastic leukemia are provoked by methotrexate and other chemotherapeutics and mediate chemoresistance. Int J Cancer 2016;138:1645–56.
24. Rots MG, Pieters R, Peters GJ, Noordhuis P, van Zantwijk CH, Kaspers GJ, et al. Role of folylpolyglutamate synthetase and folylpolyglutamate hydrolase in methotrexate accumulation and polyglutamylation in childhood leukemia. Blood 1999;93:1677–83.
25. Quesnel-Vallières M, Jewell S, Lynch KW, Thomas-Tikhonenko A, Barash Y. MAJIQlopedia: an encyclopedia of RNA splicing variations in human tissues and cancer. Nucleic Acids Res 2024;52:D213–1.
26. Traven A, Heierhorst J. SQ/TQ cluster domains: concentrated ATM/ATR kinase phosphorylation site regions in DNA-damage-response proteins. Bioessays 2005;27:397–407.
27. Johnson JL, Yaron TM, Huntsman EM, Kerelsky A, Song J, Regev A, et al. An atlas of substrate specificities for the human serine/threonine kinome. Nature 2023;613:759–66.
28. Bradley RK, Anczuków O. RNA splicing dysregulation and the hallmarks of cancer. Nat Rev Cancer 2023;23:135–55.
29. Zhou Y, Han C, Wang E, Lorch AH, Serafin V, Cho BK, et al. Posttranslational regulation of the exon skipping machinery controls aberrant splicing in leukemia. Cancer Discov 2020;10:1388–409.
30. Leclair NK, Brugiolo M, Urbanski L, Lawson SC, Thakar K, Yurieva M, et al. Poison exon splicing regulates a coordinated network of SR protein expression during differentiation and tumorigenesis. Mol Cell 2020;80:648–65.e9.
31. Byron SA, Van Keuren-Jensen KR, Engelthaler DM, Carpten JD, Craig DW. Translating RNA sequencing into clinical diagnostics: opportunities and challenges. Nat Rev Genet 2016;17:257–71.
32. Reglero C, Dieck CL, Zask A, Forouhar F, Laurent AP, Lin WHW, et al. Pharmacologic inhibition of NT5C2 reverses genetic and nongenetic drivers of 6-MP resistance in acute lymphoblastic leukemia. Cancer Discov 2022;12: 2646–65.
33. Ishikawa H. Mizoribine and mycophenolate mofetil. Curr Med Chem 1999;6: 575–97.
34. Morgado-Palacin I, Day A, Murga M, Lafarga V, Anton ME, Tubbs A, et al. Targeting the kinase activities of ATR and ATM exhibits antitumoral activity in mouse models of MLL-rearranged AML. Sci Signal 2016;9:ra91.